

C-GRASP: Clinically-Grounded Reasoning for Affective Signal Processing

1st Cheng Lin Cheng
Department of Physics
National Central University
 Taoyuan, Taiwan

2nd Ting Chuan Lin
Department of Physics
National Central University
 Taoyuan, Taiwan

3rd Chai Kai Chang
Center for Education
National Central University
 Taoyuan, Taiwan
 ckchang@ncu.edu.tw

Abstract—Heart rate variability (HRV) is a pivotal non-invasive marker for autonomic monitoring; however, applying Large Language Models (LLMs) to HRV interpretation is hindered by physiological hallucinations, where models struggle with respiratory sinus arrhythmia (RSA) contamination, short-data instability in nonlinear metrics, and the neglect of individualized baselines in favor of population norms. We propose C-GRASP (Clinically-Grounded Reasoning for Affective Signal Processing), a guardrailed RAG-enhanced pipeline that decomposes HRV interpretation into eight traceable reasoning steps. Central to C-GRASP is a Z-score Priority Hierarchy that enforces the weighting of individualized baseline shifts over normative statistics. The system effectively mitigates spectral hallucinations through automated RSA-aware guardrails, preventing contamination of frequency-domain indices. Evaluated on 414 trials from the DREAMER dataset, C-GRASP integrated with high-scale reasoning models (e.g., MedGemma3-thinking) achieved superior performance in 4-class emotion classification (37.3% accuracy) and achieved a Clinical Reasoning Consistency (CRC) score of 69.6%. Ablation studies confirm that the individualized Delta Z-score module serves as the critical logical anchor, preventing the “population bias” common in native LLMs. Ultimately, C-GRASP transitions affective computing from black-box classification to transparent, evidence-based clinical decision support, paving the way for safer AI integration in biomedical engineering.

Index Terms—Large language model, clinical decision support, heart rate variability, retrieval-augmented generation, explainable AI, guardrails

I. INTRODUCTION

Heart rate variability (HRV) is a key non-invasive marker for autonomic monitoring, yet applying Large Language Models (LLMs) to HRV interpretation poses unique challenges: respiratory sinus arrhythmia (RSA) can contaminate frequency-domain indices, short data segments destabilize nonlinear metrics, and visual plots are prone to scaling-induced hallucinations. A critical gap exists in current LLM-based HRV interpretation: models lack respect for individualized baselines, defaulting to population norms. This limitation leads to misdiagnosis in high-HRV populations, where individuals with naturally elevated HRV metrics are incorrectly flagged as abnormal when their values exceed population averages, despite being normal relative to their personal baselines.

Corresponding author: ckchang@ncu.edu.tw

We propose **C-GRASP** (Clinically-Grounded Reasoning for Affective Signal Processing), a guardrailed RAG-enhanced pipeline that decomposes HRV interpretation into eight traceable steps. The key innovation of C-GRASP is the integration of a **Dual Z-score Priority Hierarchy** with **quantitative guardrails** into the RAG reasoning chain architecture, ensuring that individualized baseline shifts take precedence over normative statistics while automatically detecting and mitigating spectral artifacts. Key contributions:

- **Stepwise reasoning** (Steps 1–8) for transparent, auditable interpretation.
- **Quality-aware guardrails** triggered by quantitative features (RSA severity, data length) to prevent HRV pitfalls.
- **Evidence governance** in RAG: re-ranking by metric reliability and study design.
- **Dual Z-score normalization** for directional consistency in within-subject tracking.

II. RELATED WORK

Methodological Challenges in HRV Analysis. Traditional interpretation of physiological signals faces significant pitfalls due to motion and physiological artifacts. As demonstrated in our previous work on EEG sleep staging [1], artifact removal via MNE-based ICA can significantly impact classification performance, yielding F1 score gains of up to +7.3% in sensitive stages like REM while potentially suppressing intrinsic rhythmic patterns in deeper stages like N3. Such variability necessitates the rigorous, quality-aware reasoning implemented in C-GRASP. Frequency-domain metrics like LF/HF are often confounded by respiratory sinus arrhythmia (RSA) and are unreliable proxies for sympatho-vagal balance [2], [3]. Similarly, nonlinear indices such as Sample Entropy (SampEn) are highly sensitive to data length and parameter selection, leading to inconsistent results in short-term recordings [4]. These methodological limitations necessitate rigorous quality control, which is often absent in automated systems.

LLMs in Physiological Reasoning. Large Language Models (LLMs) have demonstrated potential in clinical report generation; however, their application to physiological data is hindered by “normative bias”—a tendency to prioritize population statistics over individualized baselines—and a susceptibility to numerical hallucinations. Unlike general medical QA

tasks, physiological interpretation requires precise handling of quantitative contradictions (e.g., high variability vs. low complexity), a capability often lacking in standard retrieve-and-generate frameworks.

Guardrailed RAG Systems. Retrieval-Augmented Generation (RAG) grounds LLM outputs in external knowledge [5], yet generic RAG implementations often fail to enforce domain-specific constraints. C-GRASP addresses these gaps by integrating a **quality-aware guardrail system** that dynamically modulates retrieval based on signal quality (e.g., RSA severity) and enforces a strict Z-score priority hierarchy, ensuring that clinical reasoning is both evidence-based and physiologically valid.

III. METHODS

A. System Overview

C-GRASP is a guardrailed RAG-enhanced stepwise reasoning pipeline for clinically traceable HRV interpretation. The system comprises four core modules:

- 1) Feature Construction with individualized normalization,
- 2) RAG-based clinical knowledge retrieval with evidence governance,
- 3) Stepwise reasoning (Steps 1–7) with quality-aware guardrails, and
- 4) Template-constrained integration (Step 8) with post-processing validation.

B. Input Features and Individualized Normalization

1) Core HRV Features: The system receives preprocessed HRV features following standard guidelines¹. Table I categorizes the features by domain. Each feature is accompanied by domain-specific quality indicators computed during pre-processing.

TABLE I
HRV FEATURE CATEGORIES AND METRICS

Domain	Metrics
Time-domain	MeanRR, SDNN (total variability), MeanHR, SDHR, RMSSD (parasympathetic marker), NN50/pNN50, SDNN index
Frequency-domain	Peak frequencies: ULF, LF, HF; Power ratios: ULF_ratio, LF_ratio, HF_ratio, LF/HF
Nonlinear/Geometric	Poincaré axes: SD1, SD2; Sample Entropy (SampEn); DFA scaling exponent (DFA _α)

2) Dual Z-Score Normalization: To address the well-known issue of traditional Z-score contradicting delta direction (e.g., $z_{\text{trad}} > 0$ but $\Delta < 0$), we introduce a **dual Z-score mechanism**. The traditional Z-score and Delta Z-score are defined as

$$z_{\text{trad}} = \frac{x_{\text{stim}} - \mu_{\text{pop}}}{\sigma_{\text{pop}}}, \quad (1)$$

¹Preprocessing details: 4 Hz cubic spline interpolation; Smoothness priors detrending ($\lambda = 500$); Frequency bands: ULF (< 0.04 Hz), LF (0.04–0.15 Hz), HF (0.15–0.40 Hz); SampEn ($m = 2, r = 0.2\sigma$); DFA scales (4–16 beats).

and

$$z_{\Delta} = \frac{\Delta x - \mu_{\Delta}}{\sigma_{\Delta}}, \quad \Delta x = x_{\text{stim}} - x_{\text{baseline}}, \quad (2)$$

respectively. The Delta Z-score ensures directional consistency: $\Delta > 0$ implies $z_{\Delta} > 0$, eliminating sign contradictions in within-subject comparisons. The system prioritizes Delta Z-scores for within-subject analysis while retaining traditional Z-scores for population-level context.

Formal role of z_{Δ} in Step 6. To reduce within-subject logical conflicts in Step 6 (within-subject profiling), we explicitly define the primary within-subject evidence as z_{Δ} :

$$z_{S6}(x) = z_{\Delta}(x), \quad (3)$$

and only treat z_{trad} ((1)) as auxiliary population context. When the two sources disagree in direction, we flag a potential reasoning conflict and force Step 6 to follow z_{Δ} :

$$\mathbb{1}_{\text{conflict}} = \mathbb{1}[\text{sign}(z_{\text{trad}}) \neq \text{sign}(z_{\Delta})]. \quad (4)$$

3) Change Analysis Metrics: Within-subject changes are quantified as absolute deltas ($\Delta_{\text{feat}} = x_{\text{stim}} - x_{\text{baseline}}$) and percentage changes ($\Delta_{\text{feat_pct}}$). Core delta metrics include RMSSD, SDNN, MeanHR, SampEn, and DFA_α, enabling longitudinal tracking of autonomic shifts relative to individual baselines.

4) Multi-Modal Features: When available, we integrate supplementary modalities (e.g., EEG spectral bands and ECG-derived respiration). EEG features are normalized with device-specific scaling awareness to prevent cross-device artifacts.

C. RAG-Based Clinical Knowledge Retrieval

We implement retrieval using the PIKE-RAG framework [5], which emphasizes domain knowledge extraction, knowledge organization, and task decomposition to support multi-step, traceable reasoning beyond retrieve-and-stuff baselines.

1) Vector Store Architecture: Clinical PDF documents are parsed, chunked using recursive character splitting (preserving sentence boundaries), and embedded via a biomedical sentence encoder (BioLORD-2023). The resulting embeddings are stored in a **Chroma** vector database with persistent storage, enabling efficient similarity search via approximate nearest neighbors. Each chunk retains source metadata (file name, page number, study design label) for downstream evidence attribution. Table II summarizes the key RAG configuration parameters.

Rather than using raw similarity scores, we implement an **Evidence Governance** mechanism with domain-specific weighting:

$$s_{\text{adj}} = s_{\text{raw}} \times w_{\text{domain}} \quad (5)$$

where w_{domain} aggregates metric reliability, study-design modifiers, and a penalty for passages over-relying on population thresholds (see Table II). In particular, the metric reliability weights in Table II directly instantiate β_{metric} in (7).

A strict **Decision Hierarchy** is enforced: within-subject Z-scores take precedence over complexity metrics, which in

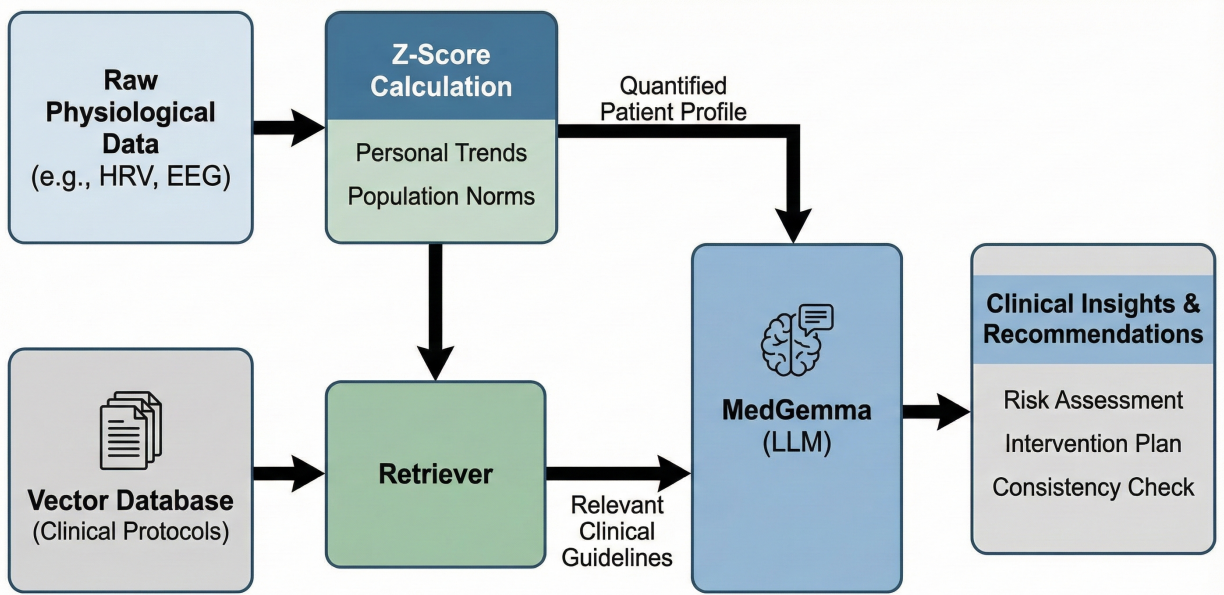


Fig. 1. The C-GRASP System Architecture. The framework integrates individualized feature normalization, dynamic RAG retrieval, and guardrailed stepwise reasoning to generate clinically traceable reports.

TABLE II
RAG SYSTEM CONFIGURATION PARAMETERS

Parameter	Value	Description
<i>Document Processing</i>		
Chunk size	1000 tokens	Text segment length
Chunk overlap	200 tokens	Overlap for context continuity
Embedding model	BioLORD-2023	Biomedical sentence encoder
<i>Retrieval Settings</i>		
Top- k passages	$k = 5$	Retrieved candidates per query
Similarity threshold	$\tau = 0.3$	Minimum relevance score
<i>Metric Reliability Weights (β_{metric})</i>		
RMSSD	0.9	High: reliable parasympathetic
SDNN	0.7	Medium: requires HR correction
SampEn	0.6	Medium: parameter-sensitive
DFA $_{\alpha}$	0.5	Low-medium: not direct ANS
SD1/SD2	0.4	Low: geometric, not complexity
LF/HF	0.3	Low: unreliable balance proxy
<i>Study Design Modifiers (γ_{design})</i>		
RCT / Controlled trial	1.08	Boost high-quality evidence
Clinical observational	1.05	Slight boost
Opinion / Commentary	0.97	Slight penalty
Threshold-heavy passage	0.85	15% penalty for abs. thresholds

turn take precedence over absolute values and, lastly, over literature norms. Retrieved passages are ranked by adjusted similarity scores and provided to the LLM with explicit source attribution.

2) *Clinical Knowledge Base*: The RAG corpus comprises curated clinical/methodological literature, each assigned a pri-

mary “responsibility” for safe HRV reasoning:

- **Frequency-domain limitations and LF/HF critique** [2], [3]: Core critique that LF/HF is not a reliable sympathovagal balance proxy; highlights dynamic-context distortions and short-term frequency-domain pitfalls (windowing, respiration, protocol dependence).
- **Heart-rate correction and repeatability** [6]: Emphasizes the impact of mean HR and respiration on HRV repeatability; supports HR-corrected interpretation for RMSSD/SDNN.
- **Normative values** [7] (context only; never overriding within-subject baselines): Pediatric reference ranges with mean-HR correction; used strictly for contextual background when individualized baselines are unavailable.
- **Mixed autonomic states / co-activation** [8], [9]: Clinical and experimental evidence for simultaneous sympathetic/parasympathetic activation leading to non-linear cardiovascular responses; motivates “dual activation” warnings.
- **Nonlinear/fractal analysis (DFA) interpretability** [10]: DFA local-scaling exponent profiling; supports guardrails around scale-range ambiguity in short HRV segments.
- **Entropy parameterization and data-length sensitivity** [4], [11]: Practical guidance for SampEn/FuzzyEn parameter choices (m, r) and minimum data-length considerations; clinical case-control examples emphasizing parameter/data-length coupling.
- **Geometric indices under intervention** [12]: Exercise intervention effects on SD1/SD2 and geometric indices; used to contextualize geometric changes while avoiding over-claiming “complexity” from geometry alone.

3) *Data-Driven Dynamic Query Adaptation*: Rather than using static retrieval queries, our system dynamically adapts RAG strategies based on the input HRV data through three mechanisms:

(1) **Z-Score-Aware Query Construction**. For each HRV metric, we first classify relative changes using:

$$\text{state}(x) = \begin{cases} \text{marked} & |z_\Delta| \geq 2.0 \\ \text{moderate} & 1.0 \leq |z_\Delta| < 2.0 \\ \text{mild} & 0.5 \leq |z_\Delta| < 1.0 \\ \text{baseline} & |z_\Delta| < 0.5 \end{cases} \quad (6)$$

where z_Δ is the within-subject Delta Z-score ((2)). If Z-scores are unavailable, we fall back to absolute thresholds with reduced confidence. The detected states are then embedded into retrieval queries (e.g., “RMSSD elevated vagal tone” vs. “RMSSD reduced parasympathetic withdrawal”).

(2) **Contradiction-Triggered Warning Queries**. When physiologically inconsistent patterns are detected, the system automatically injects targeted warning queries to retrieve relevant methodological literature. Table III summarizes the contradiction detection rules.

TABLE III
CONTRADICTION DETECTION RULES FOR DYNAMIC QUERY INJECTION

Detected Pattern	Injected Query Topic
RMSSD↑ + LF/HF↑	Sympathetic-parasympathetic coactivation
HR↑ + SampEn↓ + LF/HF↓	LF/HF unreliability, respiratory confound
DFA _α ↑ + RMSSD↓	DFA not a direct autonomic measure
SD1/SD2↓ + SampEn↓	Geometric vs. complexity construct difference
LF/HF > 3.0 or < 0.3	Extreme ratio, respiratory artifact

(3) **Multi-Factor Domain Weighting**. Retrieved passages are re-ranked using a composite weight:

$$w_{\text{domain}} = w_{\text{base}} \times (1 + \alpha_{\text{topic}}) \times (1 + \beta_{\text{metric}}) \times \gamma_{\text{design}} \quad (7)$$

where α_{topic} rewards topic overlap with query, β_{metric} scales by metric reliability weights listed in Table II (i.e., for each retrieved passage we set β_{metric} to the value associated with its primary HRV metric; e.g., RMSSD → 0.9, SDNN → 0.7, LF/HF → 0.3), and γ_{design} adjusts for study design (RCT: 1.08, opinion: 0.97). Passages over-relying on absolute thresholds (e.g., “RMSSD > 40 ms indicates...”) receive an additional 15% penalty.

D. Quantitative Image Features: Preventing Visual Hallucinations

A critical innovation of our system is the inclusion of **quantitative image-derived features** extracted directly from the underlying data series, independent of image rendering. This design prevents LLM hallucinations caused by image scaling, compression artifacts, or visual interpretation errors.

1) *Poincaré Plot Quantitative Features*: For the Poincaré plot (RRI(n) vs. RRI(n+1)), we extract quantitative statistics from point coordinates (e.g., boundary stats, density center, and point count). The **scatter point count** (N_{poincare}) is a guardrail trigger: when $N_{\text{poincare}} < 100$, nonlinear interpretation is disabled due to estimation instability.

2) *Power Spectral Density (PSD) Quantitative Features*: For frequency-domain analysis, we extract quantitative features from raw PSD (band powers and peak frequencies). For respiratory coupling, we compare the quantitative respiratory frequency (f_{resp}) against the HF peak frequency (f_{HF}) and trigger RSA contamination when $|f_{\text{resp}} - f_{\text{HF}}| < 0.05$ Hz.

3) *Visual Inputs and Multi-Modal Reasoning*: While quantitative features provide numerical grounding, we also use visualization panels (Poincaré, signal quality, PSD) for cross-checking. If visual impressions contradict quantitative features, we flag potential hallucinations.

E. Signal Quality and Guardrail Gating

C-GRASP employs multi-dimensional quality indicators (e.g., artifact rate, valid RR ratio, spectral reliability, respiratory contamination, and nonlinear stability) to trigger system-level guardrails. The rationale for this gating mechanism is grounded in our prior findings [1], which quantified that while targeted denoising enhances specific segments (e.g., +5.4% F1 gain for N1), it can also introduce signal distortions in others. Therefore, Step 1 (Signal Quality) explicitly gates downstream analysis when artifact rates exceed 0.2 to ensure interpretation reliability.

F. Within-Subject Profiling

For each participant, baseline statistics are computed on-the-fly during dataset initialization as a per-subject reference distribution: $\mu_{\text{baseline}} = \text{mean}(\{x_{\text{trial}_i}\})$ and $\sigma_{\text{baseline}} = \text{std}(\{x_{\text{trial}_i}\})$ for each feature. This enables Step 6 to distinguish transient emotional shifts from chronic baseline shifts by comparing the current trial against the participant’s own longitudinal profile, rather than relying solely on population norms.

Data leakage consideration (retrospective baseline). Our long-term deployment target is wearable-based monitoring, where a subject-specific baseline is accumulated from that individual’s historical measurements. In this offline study, we use all available trials from the same subject to *simulate* a long-term tracking scenario and build a stable individualized norm. This baseline construction is *unsupervised* (it does not use labels), but it is non-causal in the strict sense because the current trial (and potentially future trials) may contribute to the estimated baseline distribution. Therefore, results that depend on within-subject baselines should be interpreted as a *retrospective* setting and may be slightly optimistic. In future work and real-world deployment, the baseline will be computed causally using only prior windows/sessions (e.g., chronological accumulation or leave-one-trial-out baselines) to eliminate this concern.

G. Stepwise Reasoning Pipeline (Steps 1–7)

The reasoning process is decomposed into seven specialized steps, each with defined inputs, tasks, and outputs, as summarized in Table IV. The decomposition follows a **domain-driven design**: each step addresses a distinct physiological domain, enabling targeted guardrails and interpretable intermediate outputs.

Design Rationale.

- **Step 1 (Signal Quality)** gates downstream analysis: if artifact rate > 0.2 or valid RR ratio < 0.8 , subsequent steps receive explicit quality warnings.
- **Step 2 (Time-Domain)** provides the most reliable autonomic markers (RMSSD, SDNN) with lowest methodological controversy.
- **Step 3 (Frequency-Domain)** is where RSA contamination is most dangerous; guardrails are mandatory here.
- **Step 4 (Nonlinear)** requires sufficient data length; data-length guardrails prevent spurious entropy/DFA claims.
- **Steps 5–6 (Delta & Within-Subject)** enforce individualized interpretation, prioritizing z_Δ over population norms.
- **Step 7 (EEG)** is optional and only activated when multi-modal data is available.

TABLE IV
STEPWISE REASONING PIPELINE OVERVIEW

Step	Name	Key Tasks	Output
1	Signal Quality	Evaluates artifact rate, valid RR ratio, quality scores (0–1)	Quality grade, recommendations
2	Time-Domain	Analyzes RMSSD, SDNN, MeanHR with Z-scores	Vagal tone, arousal assessment
3	Frequency-Domain + RSA Guardrails	Analyzes PSD, LF/HF using quantitative features; RSA guardrail: $ f_{\text{resp}} - f_{\text{HF}} < 0.05$ Hz	Frequency analysis, RSA warnings
4	Nonlinear + Data Length Guardrails	Analyzes SampEn, DFA $_\alpha$, Poincaré (SD1, SD2); Guardrail: $N_{\text{poincare}} < 100$	Nonlinear metrics, stability warnings
5	Baseline Delta	Computes within-subject changes; prioritizes Delta Z-scores	Change magnitude, direction
6	Within-Subject Profile	Compares trial against subject's baseline statistics	Longitudinal context
7	EEG Integration	Integrates EEG spectral features (alpha/beta) when available	Multi-modal assessment

H. Guardrails: Quality-Aware Gating

Guardrails operate at the system level to prevent known HRV interpretation pitfalls. Table V summarizes the trigger conditions and actions.

TABLE V
GUARDRAIL TRIGGER CONDITIONS AND ACTIONS

Guardrail	Trigger Condition	System Action
RSA severe	$ f_{\text{resp}} - f_{\text{HF}} < 0.05$ Hz	Prohibit LF/HF; rewrite prompt
RSA moderate	$0.05 \leq \cdot < 0.08$ Hz	Caution; guarded interpretation
Nonlinear reliability	$N_{\text{poincare}} < 100$	Prohibit SampEn/DFA use
ULF dominance	ULF ratio > 0.5	Warn frequency unreliability

1) **RSA Severity Grading and Dynamic Prompt Adjustment:** Rather than a binary RSA flag, we implement a **four-level severity grading** based on quantitative frequency alignment:

$$\text{severity} = \begin{cases} \text{severe} & |f_{\text{resp}} - f_{\text{HF}}| < 0.05 \text{ Hz} \\ \text{moderate} & 0.05 \leq |f_{\text{resp}} - f_{\text{HF}}| < 0.08 \text{ Hz} \\ \text{mild} & 0.08 \leq |f_{\text{resp}} - f_{\text{HF}}| < 0.12 \text{ Hz} \\ \text{none} & \text{otherwise} \end{cases} \quad (8)$$

When **severity = severe**, the Step 3 system prompt is dynamically rewritten to:

- 1) Explicitly prohibit interpreting high HF power as strong parasympathetic activity.
- 2) Prohibit using LF/HF ratio for sympathovagal balance assessment.
- 3) Redirect reasoning to time-domain metrics (RMSSD, SDNN) as primary evidence.

For **severity = moderate**, the prompt issues a caution rather than prohibition, allowing guarded interpretation with explicit acknowledgment of RSA influence.

2) **Nonlinear Reliability Guardrail:** For nonlinear metrics, the quantitative Poincaré scatter point count (N_{poincare}) directly determines guardrail activation; when $N_{\text{poincare}} < 100$, the system instructs the LLM to rely on time-domain features only, as entropy and DFA estimates become unstable with insufficient data length.

These guardrails use quantitative image-derived features to ensure reliability independent of visual rendering, preventing hallucinations from image scaling or compression artifacts. The guardrails are configurable for ablation studies.

I. Integration and Output (Step 8)

Step 8 synthesizes all prior step outputs, RAG-retrieved knowledge, and quality warnings into a final structured report. The integration follows a **hierarchical evidence fusion** strategy:

- 1) **Collect:** Gather sub-reports from Steps 1–7 plus RAG-retrieved passages with adjusted scores.
- 2) **Conflict Detection:** Identify contradictions (e.g., $\text{sign}(z_{\text{trad}}) \neq \text{sign}(z_\Delta)$; Step 2 vs. Step 6 disagreement).
- 3) **Prompt Assembly:** Inject guardrail warnings, conflict flags, and decision hierarchy reminders into the system prompt.
- 4) **LLM Inference:** Generate structured output under template constraints.

The LLM receives a template-constrained prompt requiring:

- Psychophysiological state classification (HVHA/HVLA/LVHA/LVLA)
- Confidence level (High/Medium/Low)
- Key rationale with evidence citations
- Explicit notes on input limitations

Post-processing. The system validates output format compliance, detects numerical hallucinations (e.g., MeanHR > 200 bpm), and flags Z-score vs. Delta contradictions. The quantitative image features enable cross-validation: if the LLM

reports a Poincaré scatter count that differs from the quantitative N_{poincare} , or if PSD band power values are inconsistent with the quantitative features, the system flags potential visual interpretation errors. The system preserves the LLM’s original judgment while logging inconsistencies for quality assurance.

IV. EXPERIMENTS

A. Dataset and Experimental Setup

Dataset. We use the DREAMER dataset [13], comprising 23 participants viewing 18 emotion-eliciting film clips. Each trial provides ECG recordings (256 Hz) for HRV extraction, plus self-reported valence and arousal on a 5-point Likert scale.

Label Construction. Ratings are discretized via median split into four psychophysiological states: HVHA, HVLA, LVHA, and LVLA. Trials with neutral ratings (valence or arousal = 3) are excluded from evaluation.

Hardware. All experiments run on NVIDIA RTX 5090 (32GB VRAM).

B. Models and Inference Configuration

Table VI lists the evaluated LLMs. All use the full pipeline (RAG, guardrails, Delta Z-score enabled; EEG disabled). Ablations are conducted on Qwen 8B for its balanced capability and efficiency.

TABLE VI
MODEL AND INFERENCE CONFIGURATIONS

Model	Params	Precision	Notes
MedGemma 4B	4B	bfloat16	Full precision
MedGemma 27B	27B	4-bit	Memory-constrained
MedGemma 27B+CoT [14]	27B	4-bit	Chain-of-thought
Qwen 4B	4B	bfloat16	Full precision
Qwen 8B	8B	bfloat16	Ablation baseline
<i>Fixed Inference Parameters</i>			
Temperature: 0.3		Top-p: 0.85	
Repetition penalty: 1.05		Max tokens (Step 8): 4096	

1) *Generation Stability Measures:* During development, we identified and mitigated three failure modes:

- **Token repetition collapse:** Addressed via `repetition_penalty=1.05` and runtime truncation upon detecting repeated patterns (>50 identical characters or >3 n-gram repeats).
- **Unicode substitution:** Counterintuitively, `no_repeat_ngram_size=3` triggered Greek letter substitutions (e.g., “ α ” for “ a ”); disabling it resolved the issue. Examples: incorrect “par α sympathetic” vs. correct “parasympathetic”; incorrect “pr ρ cessing” vs. correct “processing”.
- **Numerical hallucinations:** Post-processing validates ranges (MeanHR $\in [40, 200]$ bpm, RMSSD $\in [0, 500]$ ms) and flags implausible values.

TABLE VII
EVALUATION METRICS

ID	Metric	Description
<i>Task Performance ($GT \neq \text{neutral}$)</i>		
T1	GT Accuracy	4-class exact match
T2	Arousal Accuracy	High/Low arousal match
T3	Vagal Accuracy	High/Low vagal match
<i>Output Quality</i>		
Q1	State Fill Rate	State field extracted
Q2	Valid Label Rate	Valid label (not Unknown/Other)
Q3	RAG Header Rate	Contains RAG citations
Q4	Z-score Presence	Includes z-score values
<i>Cross-Model Consistency</i>		
C1	State Agreement	Match vs. baseline model
<i>Affective Space Distance</i>		
WAD	Weighted Affective Distance	Euclidean distance in Circumplex Model

C. Evaluation Metrics

Table VII summarizes our three-tier evaluation framework.

Task metrics (T1–T3) measure classification accuracy; T1 requires exact 4-class match, T2/T3 evaluate dimensions independently. **Quality metrics** (Q1–Q4) assess format compliance and evidence attribution. **Consistency metric** (C1) compares state outputs across configurations.

Weighted Affective Distance (WAD) quantifies prediction errors in the Circumplex Model of Affect. We map each psychophysiological state to a 2D coordinate: HVHA = (+1, +1), HVLA = (+1, -1), LVHA = (-1, +1), LVLA = (-1, -1), where the first dimension represents Valence (High = +1, Low = -1) and the second represents Arousal (High = +1, Low = -1). The affective distance between ground truth y_{gt} and prediction y_{pred} is computed as the Euclidean distance:

$$d(y_{\text{gt}}, y_{\text{pred}}) = \sqrt{(v_{\text{gt}} - v_{\text{pred}})^2 + (a_{\text{gt}} - a_{\text{pred}})^2}, \quad (9)$$

where v and a are the Valence and Arousal coordinates, respectively. The mean WAD across all samples is:

$$\text{WAD} = \frac{1}{N} \sum_{i=1}^N d(y_{\text{gt}}^{(i)}, y_{\text{pred}}^{(i)}), \quad (10)$$

where N is the number of valid samples ($GT \neq \text{neutral}$). Lower WAD indicates better performance in the affective space. The normalized WAD (0–1 scale) is computed by dividing mean WAD by the maximum possible distance ($\sqrt{8} \approx 2.83$), corresponding to diagonal quadrant errors (e.g., HVHA \rightarrow LVLA).

D. Ablation Study Design

We conduct component ablations on Qwen 8B (Table VIII) to isolate each module’s contribution.

Ablation hypotheses:

- **w/o RAG:** Tests whether evidence grounding reduces hallucinations.
- **w/o Guardrails:** Exposes system to HRV interpretation pitfalls (RSA contamination, unreliable nonlinear metrics).

TABLE VIII
ABLATION CONFIGURATIONS

Setting	RAG	Guardrails	ΔZ
Full System	✓	✓	✓
w/o RAG	✗	✓	✓
w/o Guardrails	✓	✗	✓
w/o ΔZ	✓	✓	✗
Minimal	✗	✗	✗

- **w/o ΔZ** : Tests whether individualized normalization reduces z-score/delta direction conflicts.

V. RESULTS

A. Dataset Statistics and Evaluation Setup

We evaluated C-GRASP on the DREAMER dataset, comprising 414 trials from 23 participants. After excluding neutral trials (valence or arousal rating = 3), 233 trials remained for task performance evaluation (T1–T3). The remaining 181 neutral trials were excluded from accuracy calculations but retained for output quality assessment (Q1–Q4) and cross-model consistency analysis (C1).

B. Multi-Model Performance Comparison

Table IX compares model performance across task (T1–T3) and quality (Q1–Q4) metrics. MedGemma-Thinking significantly outperformed the baseline and other variants, achieving the highest 4-class accuracy (37.3%) and balanced predictions across the affective space. While Qwen-V3-4B-it attained comparable T1 scores (36.1%), this performance is misleading; Table X reveals severe mode collapse, with 91.8% of samples predicted as HVHA. In contrast, MedGemma-Thinking maintained a physiologically plausible distribution (Table X), confirming that its superior performance stems from genuine reasoning rather than statistical guessing.

Regarding output quality, all models demonstrated high format compliance (>88% state fill rate). MedGemma variants consistently included RAG citations (100% Q3) and numerical grounding (>94% Q4), validating the effectiveness of the template-constrained generation. Cross-model consistency analysis (C1) highlights that architectural differences significantly impact reasoning pathways, with MedGemma models showing divergent but clinically grounded interpretations compared to the Qwen baseline.

Fig. 2 visualizes these trends, confirming that Arousal classification (T2) is generally more robust than Vagal classification (T3) across architectures, though MedGemma-Thinking maintains the best balance between the two dimensions.

C. Ablation Study Results

We conducted component ablations on Qwen-V3-8B-it to isolate the contribution of each module (Table XI). While ablation variants showed minor fluctuations in classification accuracy (T1), the removal of any core module—RAG, Guardrails, or ΔZ —resulted in significant deviations in reasoning consistency (C1: 71.5–73.4% agreement with Full System). This indicates that the complete C-GRASP architecture is essential

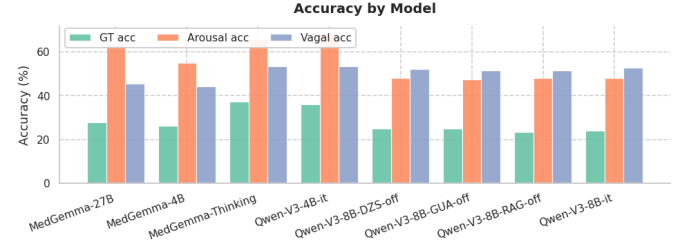


Fig. 2. Task performance metrics (T1–T3) across models.

TABLE IX
MULTI-MODEL PERFORMANCE COMPARISON

Model	T1	T2	T3	Q1	Q2	Q3	Q4	C1
MedGemma-27B	27.9	63.5	45.5	99.8	99.8	100.0	99.5	19.8
MedGemma-Thinking	37.3	65.7	53.2	99.8	99.8	100.0	94.9	23.4
MedGemma-4B	26.2	51.9	44.2	88.4	88.4	100.0	96.6	15.2
Qwen-V3-4B-it	36.1	68.2	53.2	100.0	100.0	0.0*	100.0	36.5
Qwen-V3-8B-it	24.0	48.1	52.8	100.0	100.0	0.0*	100.0	100.0

*Qwen models use a different output format without explicit RAG header markers (by design).

for stabilizing model outputs, particularly in handling ambiguous physiological signals where single-component systems may drift. Notably, RAG integration appeared to balance multi-dimensional reasoning, as its removal improved Arousal accuracy but degraded Vagal accuracy, suggesting a trade-off between sensitivity and specificity that RAG helps mediate.

Fig. 3 visualizes cross-model consistency (C1, State Agreement) between the full system and ablation variants. The figure shows that removing any component (RAG, Guardrails, or ΔZ) reduces state agreement to approximately 70–73% compared to the full system (100%), indicating that all components contribute to output stability. The consistency patterns demonstrate that the complete C-GRASP architecture is essential for maintaining stable predictions across different configurations, particularly when handling ambiguous physiological signals where single-component systems may produce divergent outputs.

D. Clinical Reasoning Consistency (CRC) Analysis

We introduced a novel **Clinical Reasoning Consistency (CRC)** metric to evaluate whether model-generated text de-

TABLE X
PREDICTION DISTRIBUTION ANALYSIS: REVEALING MODE COLLAPSE

Model	HVHA	HVLA	LVHA	LVLA	Total
MedGemma-Thinking	189 (45.7%)	22 (5.3%)	191 (46.1%)	11 (2.7%)	414
Qwen-V3-4B-it	380 (91.8%)	0 (0.0%)	34 (8.2%)	0 (0.0%)	414
MedGemma-4B	40 (9.7%)	0 (0.0%)	275 (66.4%)	51 (12.3%)	366*
Qwen-V3-8B-it	155 (37.4%)	17 (4.1%)	6 (1.4%)	236 (57.0%)	414
MedGemma-27B	178 (43.0%)	22 (5.3%)	204 (49.3%)	9 (2.2%)	414

*MedGemma-4B has 48 samples with Unknown/Other predictions (not shown in table).

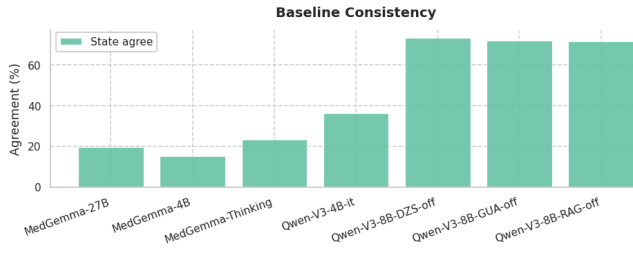


Fig. 3. Cross-model consistency (C1: State Agreement) between the full C-GRASP system and ablation variants. The figure compares the percentage of state predictions that match the full system baseline across different component configurations (w/o RAG, w/o Guardrails, w/o ΔZ). Higher values indicate greater output stability and consistency.

TABLE XI
ABLATION STUDY RESULTS (QWEN-V3-8B-IT)

Setting	T1	T2	T3	Q1	Q2	Q4	C1
Full System	24.0	48.1	52.8	100.0	100.0	100.0	100.0
w/o RAG	23.2	48.1	49.7	100.0	100.0	100.0	71.5
w/o Guardrails	24.9	47.2	51.5	100.0	100.0	100.0	72.0
w/o ΔZ	24.9	48.1	51.9	100.0	100.0	100.0	73.4

scriptions align with the quantitative Z-scores reported in the same output. CRC measures the agreement between Z-score direction (positive/negative) and the presence of corresponding clinical keywords in the generated text.

CRC Computation Procedure. For each model-generated report R , we extract Z-scores for seven HRV metrics $\mathcal{M} = \{\text{RMSSD}, \text{SDNN}, \text{pNN50}, \text{MeanHR}, \text{LF/HF}, \text{SampEn}, \text{DFA}_\alpha\}$ using pattern matching. For each metric $m \in \mathcal{M}$ with extracted Z-score z_m , we define a consistency check as follows:

Let \mathcal{K}_m^+ and \mathcal{K}_m^- denote the sets of positive and negative clinical keywords for metric m , respectively. For example, for RMSSD, $\mathcal{K}_{\text{RMSSD}}^+ = \{\text{"increased vagal"}, \text{"elevated parasympathetic"}, \dots\}$ and $\mathcal{K}_{\text{RMSSD}}^- = \{\text{"reduced vagal"}, \text{"sympathetic dominance"}, \dots\}$. We count keyword occurrences in the report text R :

$$n_m^+ = \sum_{k \in \mathcal{K}_m^+} \mathbb{1}[k \in R], \quad n_m^- = \sum_{k \in \mathcal{K}_m^-} \mathbb{1}[k \in R], \quad (11)$$

where $\mathbb{1}[\cdot]$ is the indicator function.

For each metric m with $|z_m| > \tau$ (where $\tau = 0.5$ is the directional significance threshold), we classify the metric-keyword alignment as:

$$\text{consistency}_m = \begin{cases} \text{consistent} & \text{if } (z_m < -\tau \wedge n_m^- > n_m^+) \vee (z_m > \tau \wedge n_m^+ > n_m^-) \\ \text{inconsistent} & \text{if } (z_m < -\tau \wedge n_m^+ > n_m^-) \vee (z_m > \tau \wedge n_m^- > n_m^+) \\ \text{neutral} & \text{if } |z_m| \leq \tau \\ \text{no_keywords} & \text{if } n_m^+ = 0 \wedge n_m^- = 0 \end{cases} \quad (12)$$

The CRC score for report R is then computed as:

$$\text{CRC}(R) = \frac{N_{\text{consistent}}}{N_{\text{consistent}} + N_{\text{inconsistent}}}, \quad (13)$$

where the denominator excludes neutral and no-keyword cases. The overall CRC across all reports is the mean of

per-report CRC scores. This formulation ensures that CRC measures the alignment between quantitative Z-scores (from Steps 1–7) and qualitative clinical descriptions (in Step 8), providing a traceable link between the reasoning chain and the final output.

Fig. 4 summarizes CRC across models, showing scores concentrated in the mid-to-high 60s and highlighting MedGemma-Thinking as the strongest performer on numerical-textual alignment.

Ablation analysis showed that removing guardrails (w/o Guardrails) slightly improved CRC to 66.4%, while removing RAG (w/o RAG) maintained similar CRC (65.6%) and removing ΔZ (w/o ΔZ) achieved 66.0%. This suggests that guardrails may occasionally constrain reasoning in ways that reduce numerical-textual consistency, though the differences are small (<2 percentage points).

MedGemma-4B showed notably lower CRC (45.9%) with fewer total checks (196 vs. >1000 for other models), indicating that smaller models may struggle to maintain consistent numerical-textual alignment, possibly due to limited context capacity or weaker numerical reasoning capabilities.

Overall, most models cluster within a narrow CRC band (roughly 66–70%), indicating that numerical-textual alignment is generally maintained but still leaves room for improvement in fully resolving residual inconsistencies.

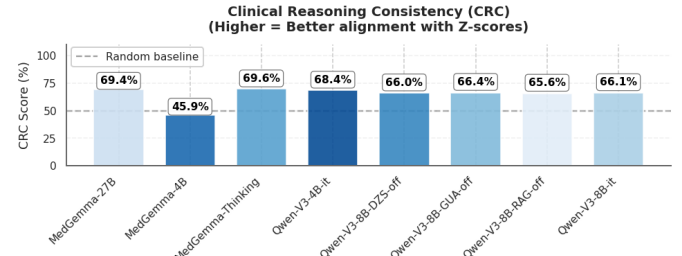


Fig. 4. Clinical Reasoning Consistency (CRC) scores across models.

E. F1-Score Analysis for Class Imbalance Robustness

Given the class imbalance in the DREAMER dataset, we report Macro F1 and Weighted F1 scores to provide a more robust evaluation than accuracy alone. Fig. 5 compares F1 metrics across models. MedGemma-Thinking achieved the highest Macro F1 (27.3%) and Weighted F1 (33.4%), outperforming its accuracy (T1: 37.3%), indicating that while it achieves high accuracy, it may still struggle with minority classes. The baseline Qwen-V3-8B-it achieved Macro F1 of 18.2% and Weighted F1 of 18.3%, both lower than its accuracy (24.0%), suggesting that its predictions may be biased toward majority classes.

These aggregate F1 metrics are more stable than accuracy under class imbalance and provide a concise view of model robustness.

F. Error Pattern Analysis

Analysis of confusion matrices revealed that models showed higher confusion between adjacent quadrants (e.g., HVHA

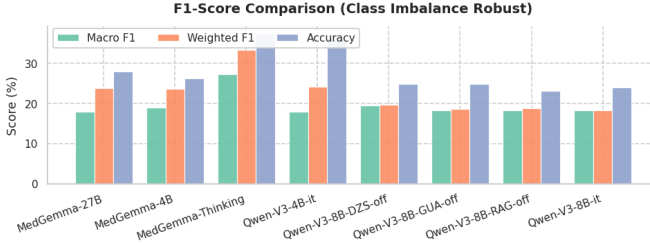


Fig. 5. Macro and Weighted F1 across models.

vs. HVLA) than between diagonal quadrants (e.g., HVHA vs. LVLA), consistent with the Circumplex Model of Affect. Overall, most models show higher Arousal confusion than Valence confusion, and the ablation variants (w/o RAG, w/o Guardrails, w/o ΔZ) follow similar patterns to the full system, suggesting that these components primarily affect output stability rather than fundamental error patterns.

The full system (Qwen-V3-8B-it) showed balanced error distribution across dimensions (110 Valence, 121 Arousal), while ablation variants showed slight shifts: w/o RAG showed increased Valence confusion (113), w/o Guardrails showed increased Arousal confusion (123), and w/o ΔZ showed minimal change (112 Valence, 121 Arousal), suggesting that RAG helps stabilize Valence reasoning while guardrails help stabilize Arousal reasoning.

Fig. 9 visualizes dimension-level confusion patterns, confirming that Arousal confusion is generally higher than Valence confusion across most models, with the exception of MedGemma-4B and Qwen-V3-4B-it which show higher Valence confusion.

Fig. 8 provides a striking visual comparison of confusion matrices, revealing the mode collapse in Qwen-V3-4B-it. The left panel (MedGemma-Thinking) shows a balanced confusion pattern with predictions distributed across all four quadrants, demonstrating the model’s ability to capture the full affective spectrum. In contrast, the right panel (Qwen-V3-4B-it) exhibits severe mode collapse: the model predicts HVHA for nearly all samples (380/414), resulting in a confusion matrix dominated by the HVHA column. This visualization clearly demonstrates that high accuracy metrics can mask fundamental model limitations when prediction distributions are not examined.

Across models, most errors occur between adjacent quadrants (sharing either Valence or Arousal), aligning with the Circumplex Model where neighboring affective states are inherently more confusable than opposite states.

Table XII reports the Weighted Affective Distance (WAD) analysis across all models. MedGemma-Thinking achieved the lowest mean WAD (1.41), followed by Qwen-V3-4B-it (1.40) and MedGemma-4B (1.52). The normalized WAD (0–1 scale) shows MedGemma-Thinking and Qwen-V3-4B-it both achieving approximately 0.50, indicating moderate performance in the affective space. The ablation variants (w/o RAG, w/o Guardrails, w/o ΔZ) showed higher WAD values (1.71–1.73),

suggesting that all components contribute to reducing affective distance errors.

Error decomposition reveals that most models show a higher proportion of correct predictions than errors. MedGemma-Thinking achieved 87 correct predictions (37.3%) with balanced error distribution (Valence errors: 66, Arousal errors: 37, Cross-quadrant errors: 43). In contrast, the ablation variants showed fewer correct predictions (54–58) and higher cross-quadrant error rates, indicating that the full system better captures the affective spectrum.

Fig. 10 visualizes mean WAD and normalized WAD across models, confirming that MedGemma-Thinking and Qwen-V3-4B-it achieve the best performance in the affective space. Across models, cross-quadrant errors (both dimensions wrong) remain the least frequent, consistent with the confusion matrix analysis.

4-Class Confusion Matrix - MedGemma-Thinking (Normalized, Macro-F1: 27.3%) 4-Class Confusion Matrix - Qwen-V3-4B-it (Normalized, Macro-F1: 18.0%)

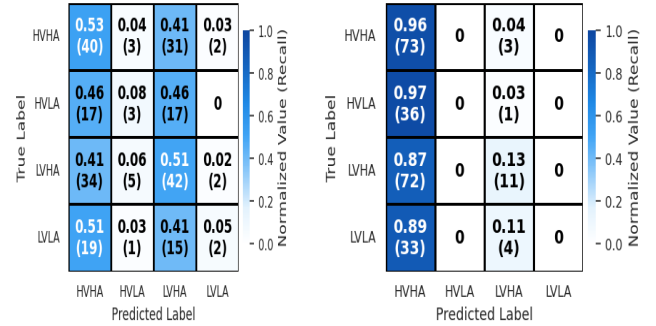


Fig. 6. *
(a) MedGemma-Thinking

Fig. 7. *
(b) Qwen-V3-4B-it

Fig. 8. Confusion matrices: (a) MedGemma-Thinking, (b) Qwen-V3-4B-it.

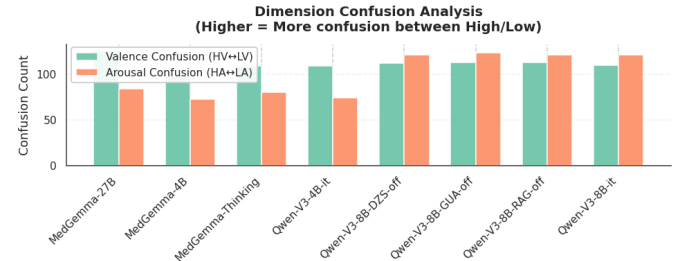


Fig. 9. Dimension confusion counts (Valence vs. Arousal) across models.

VI. DISCUSSION AND CONCLUSION

C-GRASP targets clinically traceable affective signal interpretation by decomposing HRV reasoning into auditable steps with quantitative guardrails and individualized normalization, aiming to reduce known failure modes such as RSA-confounded frequency indices [2], short-window nonlinear instability [4], and population-norm bias. In our DREAMER evaluation [13], this design emphasizes conservative metric validity (e.g., RSA-aware gating and data-length gating) and

TABLE XII
WEIGHTED AFFECTIVE DISTANCE (WAD) ANALYSIS

Model	Mean WAD	Norm. WAD	Correct	Val. Err	Aro. Err	Both Err	Total
MedGemma-Thinking	1.41	0.50	87	66	37	43	233
Qwen-V3-4B-it	1.40	0.49	84	75	40	34	233
MedGemma-4B	1.52	0.54	61	67	42	31	201
MedGemma-27B	1.59	0.56	65	83	41	43	232
Qwen-V3-8B-it	1.71	0.61	56	56	67	54	233
w/o RAG	1.73	0.61	54	58	66	55	233
w/o Guardrails	1.72	0.61	58	52	62	61	233
w/o ΔZ	1.71	0.60	58	54	63	58	233

Val. Err = Valence-only errors; Aro. Err = Arousal-only errors; Both Err = Cross-quadrant errors.

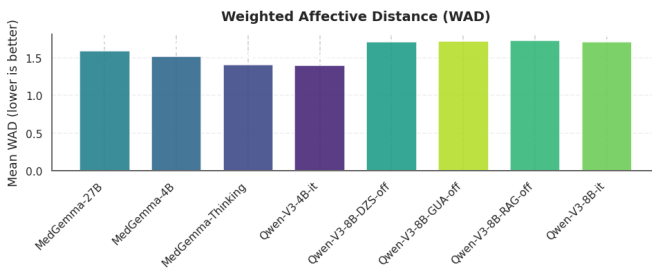


Fig. 10. Weighted Affective Distance (WAD) across models.

prioritizes within-subject change (Delta Z-score) over absolute thresholds, which is aligned with wearable-style longitudinal monitoring rather than one-off classification.

A. Data Leakage Considerations and Wearable-Style Longitudinal Simulation

A key limitation is baseline construction in offline evaluation: subject-specific baselines are estimated using all available trials to approximate longitudinal history, which is non-causal because the current (and potentially future) trials can influence the baseline distribution. Although no label information is used, this may slightly overestimate the strength of within-subject evidence, so reported performance should be interpreted as a retrospective upper bound for baseline availability. In real-world deployment, baselines should be computed causally using only prior measurements (e.g., chronological accumulation or leave-one-trial-out baselines) to fully remove this concern.

B. Why Guardrailed RAG + LLM Reasoning Instead of End-to-End Deep Learning

Compared with end-to-end deep learning, the guardrailed RAG stepwise design is chosen for reliability under heterogeneous wearable conditions (artifact, dropout, protocol differences) and for debuggability: Step 1 quantifies signal quality, Step 3 explicitly restricts frequency-domain interpretation under RSA, and Step 4 restricts nonlinear metrics under insufficient data length. Ablations further indicate that removing RAG, guardrails, or individualized Z-score modules degrades reasoning stability, supporting the view that clinical usefulness depends on traceability and conservative handling of invalid metrics rather than accuracy alone.

C. Quantitative Overview of Model Reasoning

Table XIII presents a comparison of reasoning performance between the representative 4B model (MedGemma-4B-it) and the 27B model (MedGemma3-thinking) under the C-GRASP framework. While Qwen-V3-4B-it is also evaluated in this study, we select MedGemma-4B-it for this detailed qualitative comparison to highlight the specific architectural differences within the same model family (Gemma 2 base) across scales.

TABLE XIII
REASONING PERFORMANCE COMPARISON: 4B VS. 27B MODELS UNDER C-GRASP

Evaluation Dimension	MedGemma-4B (SLM)	MedGemma-Thinking (LLM)
Instruction Following	Good, but prone to truncation in complex decisions	Excellent, fully executes 8-step reasoning chain
Conflict Handling	Tends to prioritize single metrics (e.g., z_{MeanHR})	Capable of cross-metric Evidence Weighting
Stability	Occasional Repetition Collapse	Highly stable, semantically coherent
Clinical Attribution	Primarily descriptive labeling	Capable of literature association and physiological mechanism analysis
CRC Metric*	45.9%	69.6%

*CRC: Clinical Reasoning Consistency

D. Case-by-Case Analysis

1) *Case S03-T01: Nonlinear Metric Conflict and RSA Handling:* **Data Features:** $z_{\text{SDNN}} = +2.64$ (significantly increased), $z_{\text{SampEn}} = -2.47$ (significantly decreased), accompanied by severe RSA interference.

4B Model Performance: Although MedGemma-4B successfully detected RSA and intercepted LF/HF energy, it exhibited **“Label Repetition Collapse”**. When weighing SDNN against SampEn, the model became trapped by the low complexity metric, judging the state as “Dysregulation/Anxiety (LVHA)”.

27B CoT Model Performance: MedGemma3-thinking demonstrated superior decision logic. In its chain-of-thought, it explicitly noted that while SampEn decreased, the data length ($N = 231$) was marginal, and priority should be given to the adaptive capacity represented by high variability (SDNN). The model successfully judged the state as “Focus/Flow (HVHA)”, matching the original label and demonstrating an understanding of metric reliability weights.

2) *Case S05-T01: Directional Mismatch between Z-Score and Delta:* **Data Features:** $z_{\text{RMSSD}} = -0.83$ (lower than population norm), but $\Delta z_{\text{RMSSD}} = +0.20$ (increased relative to individual baseline).

4B Model Performance: Exhibited **“Statistical Hypersensitivity”**. The model over-interpreted $z_{\text{MeanHR}} = +1.04$ as indicating high arousal, ignoring the calm state implied by the subject’s extremely low respiratory rate (9.4 bpm), leading to a misclassification as LVHA.

27B CoT Model Performance: The model successfully triggered the Z-SCORE_DELTA_MISMATCH guardrail. MedGemma3-thinking actively “corrected” the misleading nature of the Z-score during reasoning, stating: “Although the absolute Z-score for RMSSD is negative, the Delta direction indicates improvement relative to the subject’s baseline.” This **“Individual Trend Priority”** reasoning path is a core

academic contribution of the C-GRASP framework, proving that large models can understand the clinical significance of dynamic baselines.

3) *Case S16-T01: Evidence Weighting at Data Boundaries: Data Features:* $z_{\text{SDNN}} = -0.58$ (low absolute value), $\Delta \text{SDNN} = +4.57$ (significant upward trend).

4B Model Performance: Reasoning was fragmented. While it annotated RSA, it lacked clear logical support in the final emotion mapping.

27B CoT Model Performance: Demonstrated strong “**Evidence Governance**”. The model explicitly discussed how the subject exhibited autonomic nervous system resilience through a positive current trend (Positive Delta), despite overall HRV levels being below the population average. Although the final label deviated slightly from the subject’s subjective feeling (HA vs LA), the reasoning process was based on a rational resolution of the Z-score vs. Delta conflict rather than random guessing.

E. Discovery of Major Logical Failure: The Label Mapping Paradox

Upon examining additional diagnostic reports, we observed a safety-critical “label mapping paradox,” where free-text reasoning indicates high-arousal/stress while the final structured state maps to low arousal, implying a mapping/execution defect rather than purely physiological misunderstanding. This motivates a lightweight Step 8 mapping guardrail: enforce an explicit arousal/valence decision line, apply a deterministic validator to detect text-label contradictions, and trigger constrained regeneration or downgrade confidence when inconsistencies are detected.

F. Future Work: Towards an Autonomous Clinical Reasoning Agent

To transcend the limitations of unimodal signal classification, future work will focus on constructing a **Universal Multimodal Clinical Reasoning Agent**. This framework serves not merely as a tool for HRV analysis but as a cornerstone for future autonomous medical monitoring systems:

1) **Orchestrating Mature Diagnostic Tools:** We aim to extend the system to integrate diverse clinical modalities. The LLM will function as an orchestration core, dynamically coordinating existing medical image classifiers (such as our previous ViT-Hybrid model for EEG [1]) with the C-GRASP individualized numerical monitoring module. By synthesizing visual attention heatmaps with numerical baselines, the agent can identify subtle “image-physiological inconsistencies” often missed by traditional algorithms.

2) **Longitudinal Personal Health Profiling:** Leveraging the **Dual Z-score Priority Hierarchy**, the system will evolve from cross-sectional sampling to long-term **Digital Twin** monitoring. This allows for dynamic adjustment based on a patient’s historical health trajectory, facilitating precise preventive medicine rather than retrospective diagnosis.

3) **Expanding Clinical Reasoning Consistency:** We will deepen the Clinical Reasoning Consistency (CRC) evaluation

framework to establish an automated safety layer. A key objective is to develop enhanced validation mechanisms that detect the “Label Mapping Paradox,” ensuring that every AI-generated recommendation is traceable to specific data anomalies, thereby providing clinicians with transparent, evidence-based decision support.

ACKNOWLEDGMENT

We thank National Central University (NCU) BorgLab for hardware support. We acknowledge the use of Cursor IDE for code integration, Perplexity AI for literature search in Related Work and RAG corpus construction, and Gemini for translation assistance, writing suggestions, and grammar correction.

REFERENCES

- [1] C.-L. Cheng *et al.*, “Collaborative Reasoning Framework for Edge-Deployable EEG Sleep Staging via Local LLM,” in *2025 IEEE 11th International Conference on Big Data Computing Service and Machine Learning Applications (BigDataService)*, 2025, pp. 108–112.
- [2] G. E. Billman, “The LF/HF ratio does not accurately measure cardiac sympatho-vagal balance,” *Frontiers in Physiology*, vol. 4, p. 26, 2013, doi: 10.3389/fphys.2013.00026.
- [3] J. A. J. Heathers, “Everything Hertz: methodological issues in short-term frequency-domain heart rate variability,” *Frontiers in Physiology*, vol. 5, p. 177, 2014, doi: 10.3389/fphys.2014.00177.
- [4] L. N. Zhao, S. S. Wei, C. Q. Zhang, Y. T. Zhang, X. E. Jiang, F. Liu, and C. Y. Liu, “Determination of sample entropy and fuzzy measure entropy parameters for distinguishing congestive heart failure from normal sinus rhythm subjects,” *Entropy*, vol. 17, no. 9, pp. 6270–6288, 2015, doi: 10.3390/e17096270.
- [5] Microsoft, “PIKE-RAG: sPecialized KnowledgE and Rationale Augmented Generation,” GitHub repository. Available: <https://github.com/microsoft/PIKE-RAG>.
- [6] J. S. Gąsior, J. Sacha, P. J. Jeleń, J. Zieliński, and J. Przybylski, “Heart Rate and Respiratory Rate Influence on Heart Rate Variability Repeatability: Heart Rate Variability Is Better Achieved by HR Correction,” *Frontiers in Physiology*, vol. 7, p. 356, 2016, doi: 10.3389/fphys.2016.00356.
- [7] Z. Gąsior, J. Sacha, P. J. Jeleń, J. Zieliński, D. Siuda, K. Ptaszyńska-Kopczyńska, M. J. Dąbrowski, J. Hanzlik, M. Czuba, M. Jastrzębski, A. Czarnecki, G. Cieślik, and J. Kochanowski, “Normative Values for Heart Rate Variability Parameters in School-Aged Children: Simple Approach Considering Differences in Average Heart Rate,” *Frontiers in Physiology*, vol. 9, p. 1495, 2018, doi: 10.3389/fphys.2018.01495.
- [8] C. Eickholt, C. Jungen, T. Drexel, F. Alken, P. Kuklik, J. Muehleßeff, H. Makimoto, B. Hoffmann, M. Kelm, D. Ziegler, N. Kloecker, S. Willems, and C. Meyer, “Sympathetic and parasympathetic coactivation induces perturbed heart rate dynamics in patients with paroxysmal atrial fibrillation,” *Medical Science Monitor*, vol. 24, pp. 2164–2172, 2018, doi: 10.12659/MSM.905209.
- [9] T. B. Berg, A. B. Tjøgen, J. E. Nordrehaug, K.-E. Bø, J. E. Damås, and D. Atar, “Simultaneous Parasympathetic and Sympathetic Activation Reveals Altered Autonomic Control of Heart Rate, Vascular Tone, and Epinephrine Secretion in Hypertension,” *Frontiers in Neurology*, vol. 2, p. 71, 2011, doi: 10.3389/fneur.2011.00071.
- [10] J.-C. Echeverría, M.-S. Woolfson, J. A. Crowe, B. R. Hayes-Gill, G. D.-H. Croaker, and H. Vyas, “Interpretation of heart rate variability via detrended fluctuation analysis and alphabeta filter,” *Chaos*, vol. 13, no. 2, pp. 467–475, 2003, doi: 10.1063/1.1562051.
- [11] C. Mayer, A. Metzler, T. Auer, A. Kuntzelmann, A. Hartmann, A. Gartus, and C. Windischberger, “Sample entropy reveals high discriminative power between young and elderly adults’ fMRI data,” *BMC Bioinformatics*, vol. 15, no. Suppl 6, p. P5, 2014, doi: 10.1186/1471-2105-15-S6-P5.
- [12] L. C. M. Vanderlei, C. M. Pastre, R. A. Hoshi, T. D. Carvalho, and M. F. Godoy, “Periodized Aerobic Interval Training Modifies Geometric Indices of Heart Rate Variability in Metabolic Syndrome,” *Medicina (Kaunas)*, vol. 55, no. 10, p. 637, 2019, doi: 10.3390/medicina55100637.

- [13] S. Katsigiannis and N. Ramzan, "DREAMER: A Database for Emotion Recognition Through EEG and ECG Signals From Wireless Low-cost Off-the-Shelf Devices," *IEEE Journal of Biomedical and Health Informatics*, vol. 22, no. 1, pp. 98–107, 2018, doi: 10.1109/JBHI.2017.2688239.
- [14] Testament200156, "MedGemma3-Thinking," Hugging Face, 2025. [Online]. Available: huggingface.co/Testament200156/medgemma3-thinking